NAWCWPNS TP 8149

DESIGN OF ORDNANCE TO PASS THE GOLDEN FRAGMENT TEST

by

Eric Lundstrom

Ordnance Development Division
Ordnance Systems Department

AUGUST 1994

NAVAL AIR WARFARE CENTER WEAPONS DIVISION
CHINA LAKE, CA 93555-6001

Naval Air Warfare Center Weapons Division

FOREWORD

The work described in this report was performed at the Naval Air Warfare Center Weapons Division, China Lake, Calif., under the sponsorship of the Naval Sea Systems Command (Don Porada, Cognizant Technology Manager) under Project Element No. 63609N and Appropriation No. AB1741319. This report contains the results of the analysis of a standard half-inch steel cube impacting cased energetic materials at 8300 ft/s. Minimum requirements for preventing the prompt initiation of detonation are presented in tables and plots of case and liner material and thickness. Examples of ordnance design are given.

This report has been reviewed for technical accuracy by Martha Norris and Ross Heimdahl.

Approved by
D. A. GOSS, *Head*
Ordnance Systems Department
27 July 1994

Under authority of
D. B. McKINNEY
RAdm., U.S. Navy
Commander

Released for publication by
S. HAALAND
Deputy Commander for Research & Development

NAWCWPNS Technical Publication 8149

Published by ..... Technical Information Department
Collation ..... Cover, 20 leaves
First printing ..... 410 copies

REPORT DOCUMENTATION PAGE

Form Approved OMB No. 0704-0188

1. AGENCY USE ONLY (Leave blank)	2. REPORT DATE	3. REPORT TYPE AND DATES COVERED
	August 1994	Summary

4. TITLE AND SUBTITLE

DESIGN OF ORDNANCE TO PASS THE GOLDEN FRAGMENT TEST

5. FUNDING NUMBERS

Appropriation No. AB1741319

6. AUTHOR(S)

Eric Lundstrom

7. PERFORMING ORGANIZATION NAME(S) AND ADDRESS(ES)

Naval Air Warfare Center Weapons Division
China Lake, CA 93555-6001

8. PERFORMING ORGANIZATION REPORT NUMBER

NAWCWPNS TP 8149

9. SPONSORING/MONITORING AGENCY NAME(S) AND ADDRESS(ES)

Naval Sea Systems Command
Washington, D.C. 20362

10. SPONSORING/MONITORING AGENCY REPORT NUMBER

11. SUPPLEMENTARY NOTES

12a. DISTRIBUTION/AVAILABILITY STATEMENT

A statement; distribution is unlimited.

12b. DISTRIBUTION CODE

13. ABSTRACT (Maximum 200 words)

NAVSEA Instruction 8010.5 requires that Navy munitions be impacted by at least two standard fragments with no resulting hazardous case debris. Computer programs have been developed that are capable of predicting whether or not standard fragments result in detonation of the munition. The SMERF code has been applied to predict the outcome of standard fragment impact tests and the results have been generalized in the form of tables and plots that can be used as design guides. The munition case and liner materials and thickness can be chosen so that the munition will not detonate when impacted by the standard fragments. Specific examples are given.

14. SUBJECT TERMS

Insensitive Munitions, Fragment Impact, Detonation, Design, Explosive, SMERF

15. NUMBER OF PAGES

38

16. PRICE CODE

17. SECURITY CLASSIFICATION OF REPORT	18. SECURITY CLASSIFICATION OF THIS PAGE	19. SECURITY CLASSIFICATION OF ABSTRACT	20. LIMITATION OF ABSTRACT
UNCLASSIFIED	UNCLASSIFIED	UNCLASSIFIED	SAR

CONTENTS

INTRODUCTION

In order to ensure munition safety, the U.S. Navy requires that ordnance items be tested to assess their response to accidental stimuli. The basic assessment tests are described in a Military Standard (Reference 1). They include a standard fragment impact test which has become known by workers in the field as the "Golden Fragment" test. The fragment consists of a 1/2-inch, 250-grain, mild-steel cube traveling at 8300 ft/s. A number of the 1/2-inch cubes are explosively launched at the target ordnance. The test ordnance item must be struck by at least two fragments. Aiming is not very accurate; therefore, the impact points are not predictable. The orientation of the cubes has not been measured, but the author believes that a nearly flat-on orientation is probable. A passing criterion for the test is that the response of the munition is not worse than burning. That is, the energetic material may ignite and burn, and the case may rupture, but there may be no hazardous fragments projected beyond 50 feet from the test setup.

The most violent response of the target ordnance to fragment impact is detonation. With modern hydrocodes, it is feasible to predict whether or not detonation will occur as a result of fragment impact. Less violent ordnance reactions to fragment impact, such as explosion or deflagration, are still failing responses to the Golden Fragment test. Because they are more complicated phenomena than the transition to detonation, they are not amenable to predictive analysis at this time. Under many circumstances, if a munition does not detonate in response to the fragment impact test, then it will pass the test. Since the detonation response is predictable, then it makes sense to design the munition so that it will not detonate. Unacceptably violent responses other than detonation may still occur. For these, ordnance designers may rely on experience with similar energetic materials.

Criteria are derived here for choosing an energetic material that will pass the Golden Fragment test in generic ordnance configurations. The tool for generating the criteria is the Multimaterial Eulerian Reactive Flow (SMERF) computer code which is an Eulerian hydrocode that uses the zero-order variation of the Forest Fire burn law (Reference 2) for detonable energetic materials. The shock sensitivity criteria are expressed in terms of the wedge tests results which are used to calibrate the burn law. A graphical representation of this is the shock sensitivity plane (References 3 and 4) where threshold boundaries can be drawn between ordnance items that pass the Golden Fragment test and those that do not. A relation to the more common large-scale gap test measure of shock sensitivity is shown.

THE FRAGMENT IMPACT MODEL FOR COMPUTER ANALYSIS

The 1/2-inch steel cube is approximated by a 1/2-inch-long, 1/2-inch-diameter steel blunt cylinder. The cylinder is presumed to strike the test ordnance item at normal incidence and zero yaw. This is known to be the worst case. The curvature of the ordnance case is also neglected, since the fragment is so small compared to the diameter of the case. Multiple fragment effects are neglected, since they become important in the transition to detonation only when the fragments are separated by less than a few fragment diameters. The major influence on the threshold for detonation is the case thickness. Therefore, this is the focus of the investigation. It is also known that case material will have some effect on the threshold. Four case materials were chosen: steel, aluminum, titanium, and graphite-epoxy. The fragment impact geometry is shown in Figure 1.

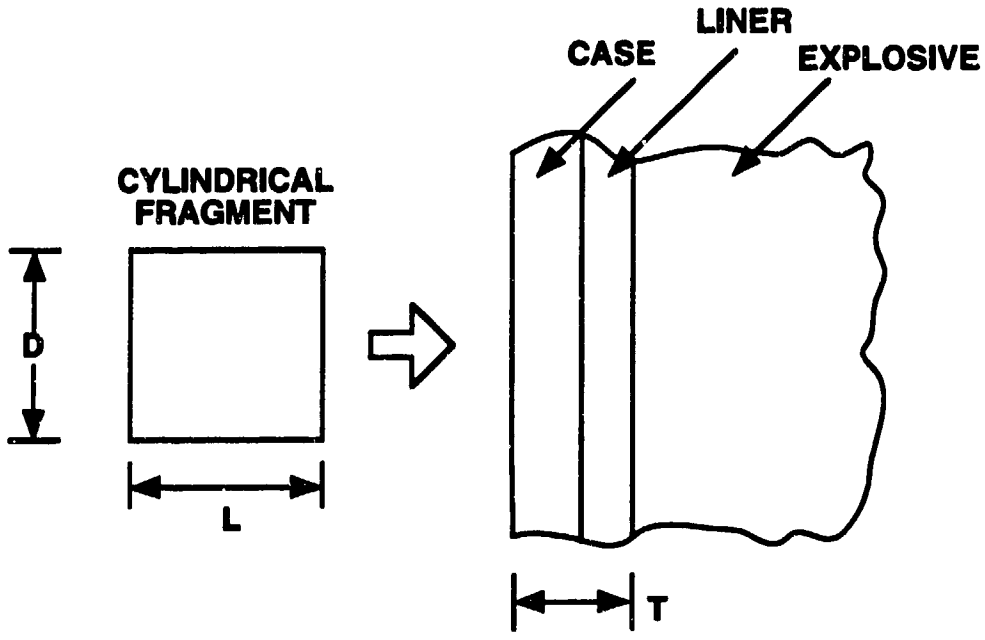

FIGURE 1. Geometry for Fragment Impact Studies (for the Golden Fragment Test, D = L = 1/2 inch and V = 8300 ft/s).

The shock Hugoniots used in the analysis for the metallic fragment and case components are for steel with a density of 7.9 g/cm^3

$$U_s = 0.45 + 2.6 \cdot U_p$$

for aluminum with a density of 2.703 g/cm^3

$$U_s = 0.535 + 1.497 \cdot U_p$$

and for titanium with a density of 4.527 g/cm^3

$$U_s = 0.4937 + 1.019 \cdot U_p$$

where U_s and U_p are the shock and particle velocities in cm/μs.

The shock Hugoniot for the graphite epoxy case was obtained from Reference 5. For a material with a density of 1.53 g/cm^3, it is

$$U_s = 0.33 + 2.2 \cdot U_p$$

Reference 5 is of particular interest because it also deals with fragment impact on cased energetic materials. It investigates more complicated case configurations, including low density layers specifically intended to mitigate initiation of detonation.

For the energetic material, the shock Hugoniot for an experimental propellant reported in Reference 4 was used. A propellant was chosen because rocket motors normally have thinner cases than warheads, and their reaction to the Golden Fragment test is very severe. The shock Hugoniot for the propellant with a density of 1.6188 g/cm^3 is given by

$$U_s = 0.22 + 2.0 \cdot U_p$$

This particular propellant was chosen because it was the subject of an extensive analytical investigation on shock sensitivity tests, and some experimental data are available. The equation of state of the energetic material is not expected to be a major influence on the results of the fragment impact calculations, since the shock Hugoniots for most energetic materials are quite similar.

The results from a sample calculation are shown in Figure 2. The case is 0.10-inch-thick graphite-epoxy. The figure displays a sequence of pressure contour plots showing the propagation through the case and into the energetic material. In response to the shock wave, the material starts to explosively decompose (burn), which increases the intensity of the shock. The process results in the formation of a detonation wave which is characterized by a particular propagation velocity and high pressure. The plots also include a contour line for 50% detonation products, which also helps to identify the transition to detonation. The example shown in Figure 2 is very close to threshold. The same fragment impacting on a slightly less shock sensitive energetic material would not lead to detonation. The pressure relief effects due to the rarefaction waves arising at the fragment edges would overcome the pressure gain due to the explosive burn, and the shock wave would decay rather than grow.

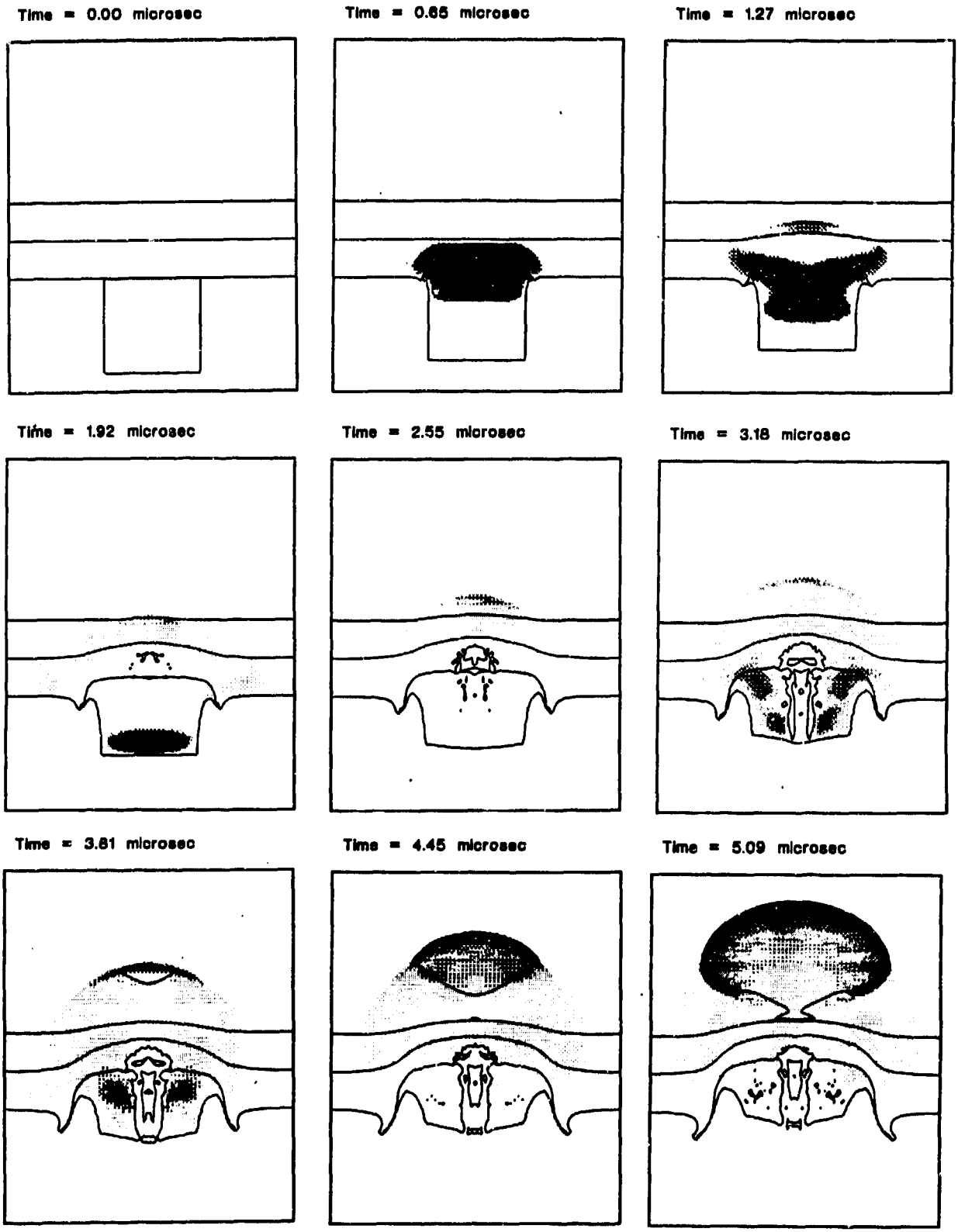

FIGURE 2. A Sequence of Pressure Contour Plots Illustrating a Transition to Detonation Near the Threshold. The case is 0.10-inch-thick graphite epoxy. The contour of 50% detonation products is included.

THE SHOCK SENSITIVITY PLANE

The shock sensitivity plane concept developed in Reference 3 is a useful way of correlating shock sensitivity effects over a wide range of energetic materials. It is also a good way to display the results of theoretical analysis when shock sensitivity is important. A review of the concept is included here.

The variation of the Forest Fire burn model used in the SMERF code has been used very successfully to predict experimental results of interest to the insensitive munitions field. These include fragment impact, which is of concern here, and sympathetic detonation. The original formulation of the Forest Fire burn model has been used in other computer codes in the analysis of a wide variety of situations in which the shock-to-detonation transition in explosives is important.

The Forest Fire burn model is calibrated solely with the results of the wedge test. In this test, a shock wave is introduced into a wedge-shaped explosive. The shock wave is observed to accelerate as a result of the decomposition of the explosive behind the shock. The space–time trajectory of the shock wave can be measured by observing the intersection of the accelerating shock wave with the diagonal face of the wedge. The major result of the wedge test is the distance that it takes for the shock wave to run up to detonation as a function of the pressure in the input shock. Log-log plots of run distance as a function of initial shock pressure are commonly made. These are called Pop plots. The run distance can very often be fit quite nicely by a straight line on the Pop plot over the range of the experimental data. An equation for this line is

$$R = (P_1/P)^S$$

where R is the run distance in centimeters, P is the shock pressure in kilobars, and S is the slope of the straight line on the Pop plot. Therefore, P_1 is the shock pressure in kilobars which will produce a run distance of one centimeter. The quantity P_1 is known as the shock sensitivity pressure.

The Pop plot slope, S, and the shock sensitivity pressure, P_1, are two numbers that are directly input into the SMERF hydrocode to characterize shock sensitivity. They are the only data required. It is natural to consider the plane formed by these two numbers. The plane is called the shock sensitivity plane and is shown in Figure 3. A point on the plane represents a straight line on the Pop plot. Conversely, the shock sensitivity of an explosive can be represented by a point on the shock sensitivity plane. In Figure 3, points representing a number of explosives are shown. Wedge test results for the explosives included in Figure 3 are summarized in Appendix A. In general, insensitive explosives have a large value of P_1.

The slope parameter controls how the explosive responds to a transient shock pressure pulse with peak pressure P_0 and a time duration, τ. If the slope is very large, then the explosive will run to detonation whenever P_0 is greater than P_1. That is, the criterion for detonation depends only on the peak pressure. For small slopes, the time duration, τ, is important. For a slope of about 1.5, the detonation criterion takes on the well-known form

$$P_0^2 \cdot \tau = \text{constant}$$

As can be seen in Figure 3, some of the most studied explosives, PBX-9404 and Composition B, have a slope S = 1.5.

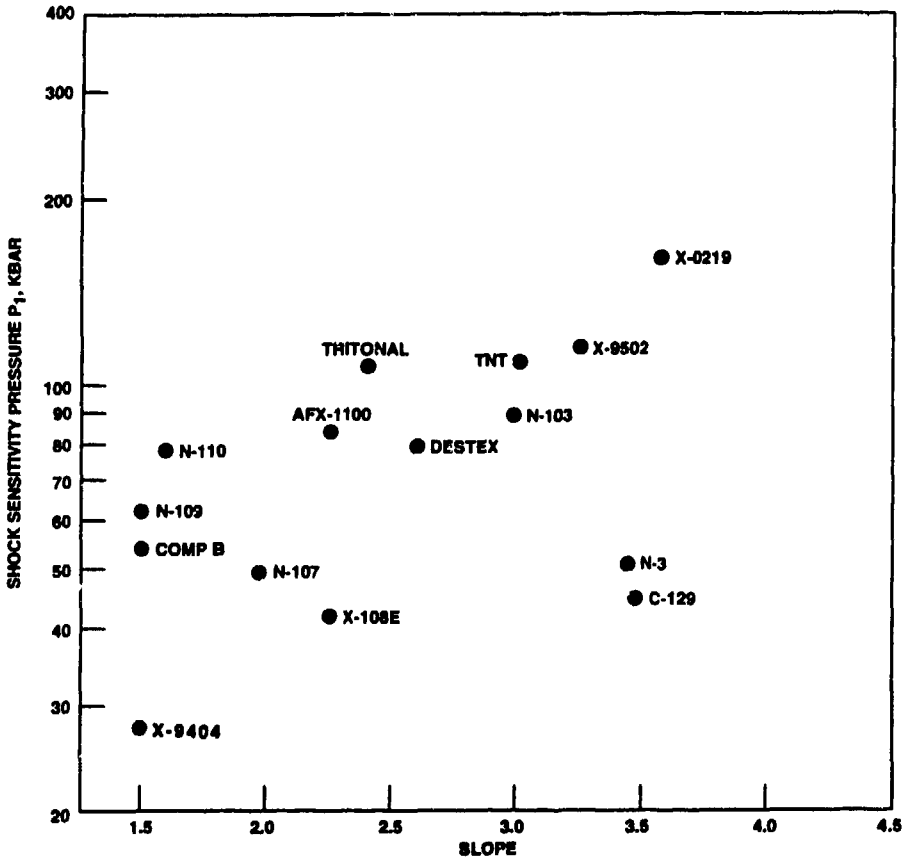

FIGURE 3. Shock Sensitivity Plane Showing Points for Several Common Explosives and Propellants.

SHOCK SENSITIVITY THRESHOLDS FOR THE GOLDEN FRAGMENT TEST

The input to the SMERF code is the shock sensitivity plane variables, S and P_1. One can run the code and observe whether the outcome is a detonation or not. If the outcome is a detonation, one can repeat the calculation for a less sensitive explosive by increasing the input value of P_1. Conversely, if the outcome is not a detonation, one can decrease P_1. Keeping S constant, one can thereby determine a threshold value of shock sensitivity which separates those explosives that detonate in the Golden Fragment test from those that do not. The SMERF code has been designed to expedite this process.

The threshold shock sensitivity for the Golden Fragment test has been calculated as a function of case material and thickness. The predicted threshold shock sensitivities are tabulated in Appendix B (Tables B-1 through B-4) for the unlined cased explosive. The tables include the values of the shock sensitivity pressure which resulted in a detonation and no detonation that bracket the threshold.

The threshold results are plotted in Figures 4, 5, and 6 for S = 1.5, 2.5, and 3.5, respectively. In each figure, the threshold value of P_1 is plotted as a function of case thickness in inches. For comparison, each figure contains the results for steel, aluminum, titanium, and graphite-epoxy cases. The effect of the Pop plot slope parameter, S, is shown for a steel cased explosive in Figure 7.

The variation of threshold value of P_1 with case thickness displays a characteristic behavior. The threshold drops slowly with thickness until the thickness is about 0.25 inches. At that point, the threshold drops much more quickly. The reason is that the relief wave originating at the cylinder circumference reaches the axis at an axial distance of about one radius. Until this point, the maximum pressure in the shock wave is constant. Thereafter, the shock pressure begins to decay very rapidly. When the case thickness is less than about one radius, then at least part of the high pressure portion of the shock wave propagates into the explosive before the relief waves converge to the axis.

It is obvious from the figures that there is not much difference in threshold with case materials for a thin case with thickness less than 0.25 inch. There seems to be more of a substantial difference between the materials for thick cases with thickness greater than 0.25 inch. This point is worth emphasizing: the threshold shock sensitivity is most strongly affected by case thicknesses greater than the fragment radius. This is shown here for the half-inch-diameter cylinder, but it also holds true for all cylinders that have a diameter greater than the critical diameter of the explosive.

There is experimental evidence that the case material may have a more substantial effect on thin cases than is indicated here. Reference 6, for example, indicates that there is a measurable change in velocity threshold for detonation that depends on the material of very thin cases. This is due to the phenomenon of shock desensitization whereby an explosive responds differently to multiple shock waves than it would to an equivalent single shock wave of the same total pressure. There is a version of the Forest Fire burn model that takes shock desensitization into account (Reference 7), but it is not implemented in the SMERF code. In any case, it is felt that it is a relatively small effect on the results of the Golden Fragment test.

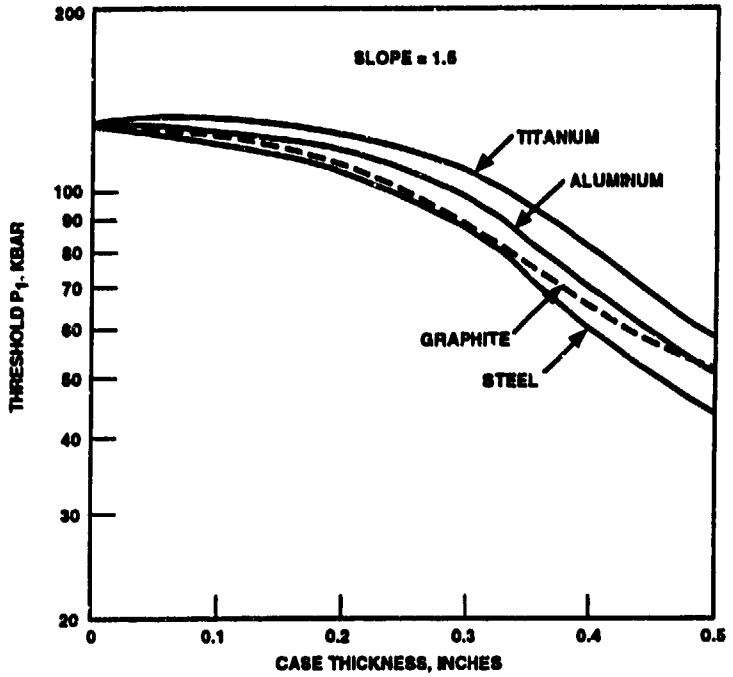

FIGURE 4. Threshold Shock Sensitivity Pressure, P_1, as a Function of Case Thickness for Slope Parameter S = 1.5.

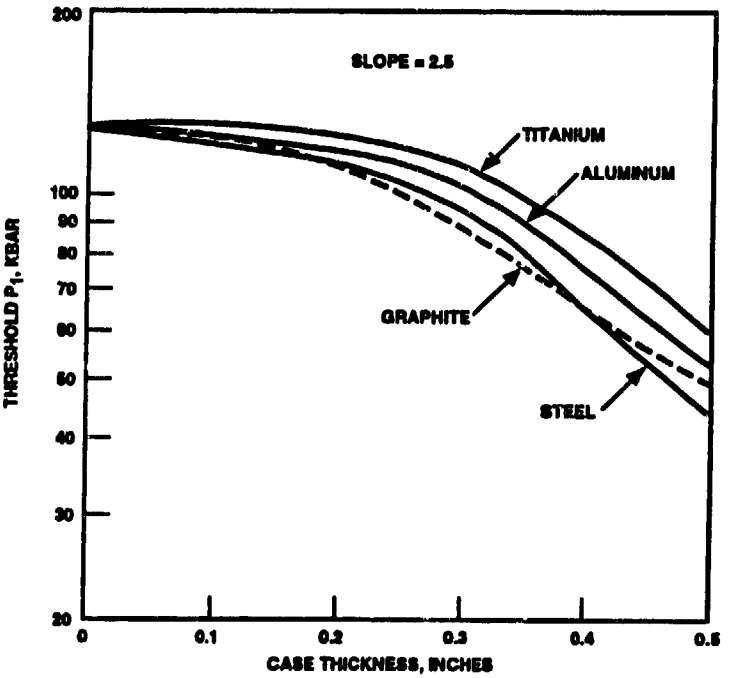

FIGURE 5. Threshold Shock Sensitivity Pressure, P_1, as a Function of Case Thickness for Slope Parameter S = 2.5.

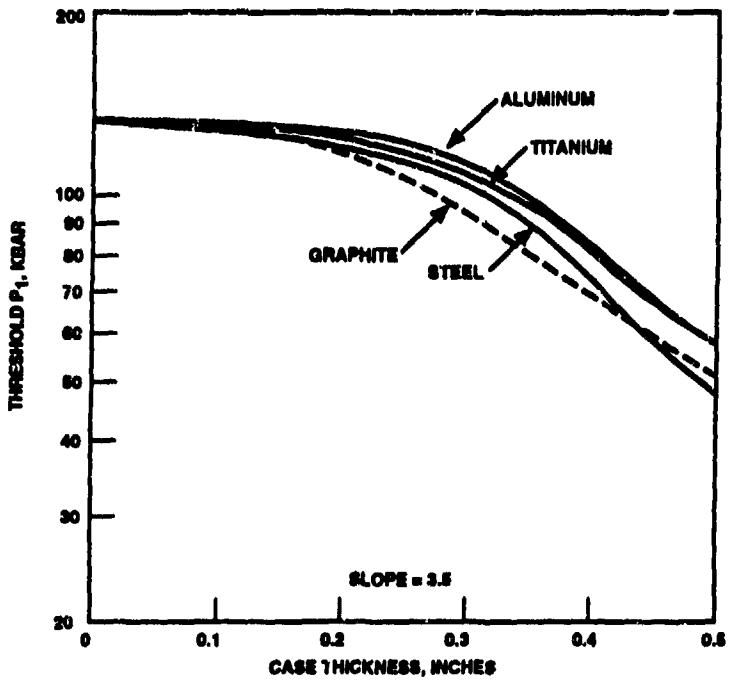

FIGURE 6. Threshold Shock Sensitivity Pressure, P_1, as a Function of Case Thickness for Slope Parameter S = 3.5.

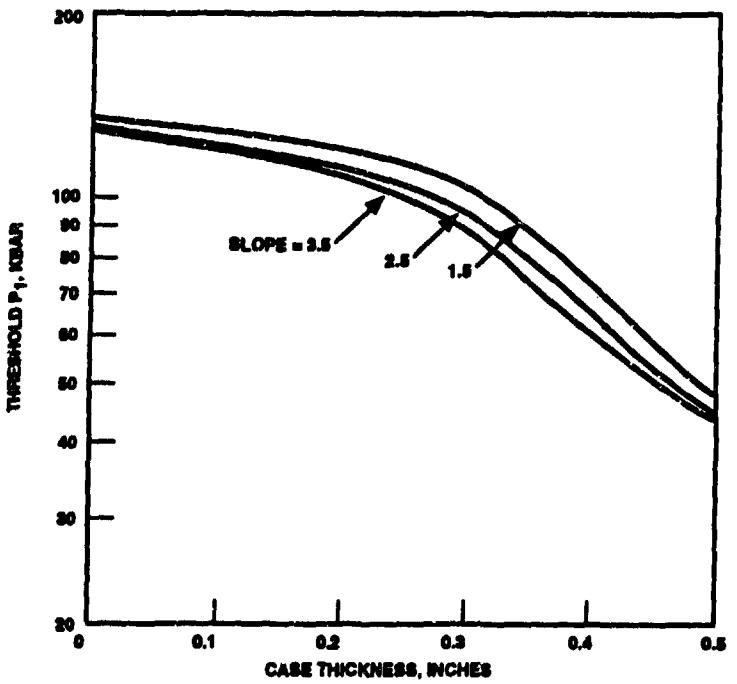

FIGURE 7. Threshold Shock Sensitivity Pressure, P_1, as a Function of Steel Case Thickness. The figure shows the effect of the Pop plot slope on the threshold.

THRESHOLD CRITERIA ON THE SHOCK SENSITIVITY PLANE

One reason for using the shock sensitivity plane in Figure 3 is that one can draw lines which separate the energetic materials that detonate in a particular test from those that do not. Figure 8 is the same as Figure 3, except that threshold shock sensitivity values for a steel-cased explosive have been replotted from Figure 7. Each line represents the threshold for a particular case thickness. If one picks a case thickness of 0.3 inch, for example, every explosive that lies above the 0.3-inch line in Figure 8 will not detonate promptly in the Golden Fragment test, and those that lie below will detonate and fail the test. The points representing the shock sensitivity of individual explosives in Figure 3 are included in Figure 8. However, for clarity, the point labels have been removed.

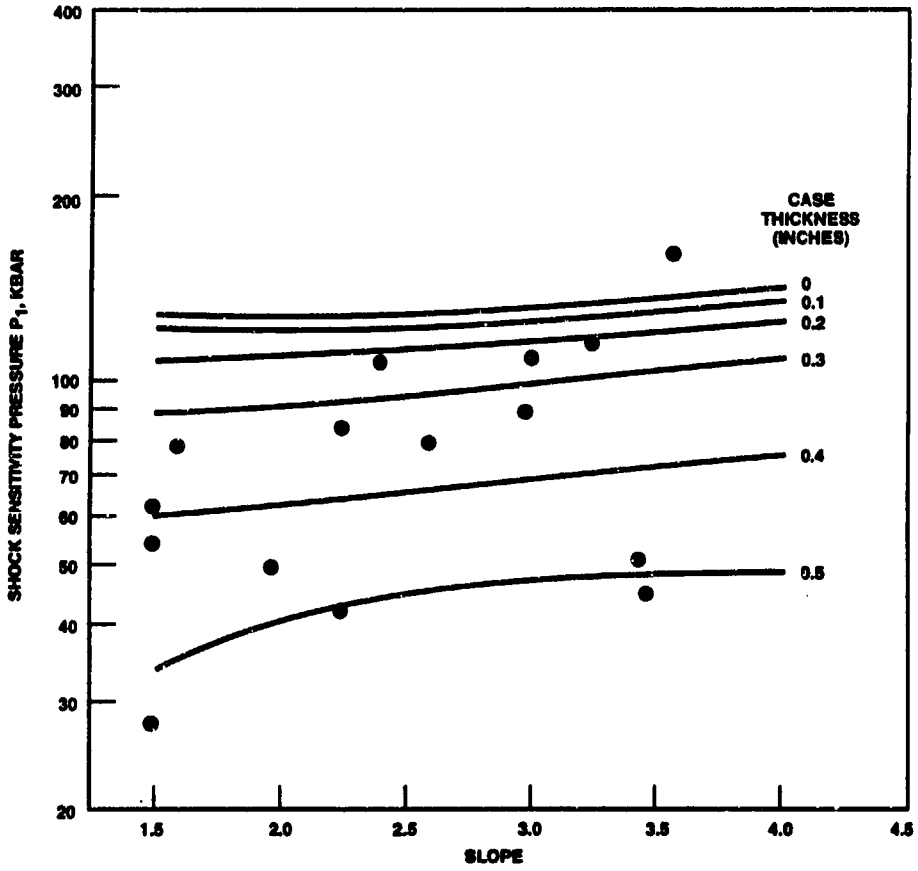

FIGURE 8. Shock Sensitivity Plane From Figure 3 Including the Threshold Curves for Fragment Impact on Steel-Cased Explosive.

If Pop plot data are available, the shock sensitivity plane shown in Figure 8 is the best place to compare shock sensitivity requirements for the Golden Fragment test with actual explosives. For example, Destex will pass the test if the case thickness is 0.4 inch and will fail if the case thickness is 0.3 inch. It can be seen that almost all main charge explosives will pass the test if the case thickness is greater than about 0.5 inch. For cases thinner than 0.5 inch, the outcome of the test depends on the shock sensitivity of the explosive. There are very few main charge explosives that will pass the test without a case for protection. Rocket motors loaded with detonable propellants can have a difficult time passing the Golden Fragment test because the motor case is usually quite thin.

Another reason for using the shock sensitivity plane is that one can compare the results from completely different tests. In References 3 and 4, for example, the results of large-scale gap tests (LSGT) were calculated using a one-dimensional hydrocode and plotted on the shock sensitivity plane. The results are reproduced in Figure 9. This figure is the same as Figure 8, except that lines representing contours of constant LSGT results are included. The numerical values of the threshold shock sensitivity for the LSGT are tabulated in Appendix C.

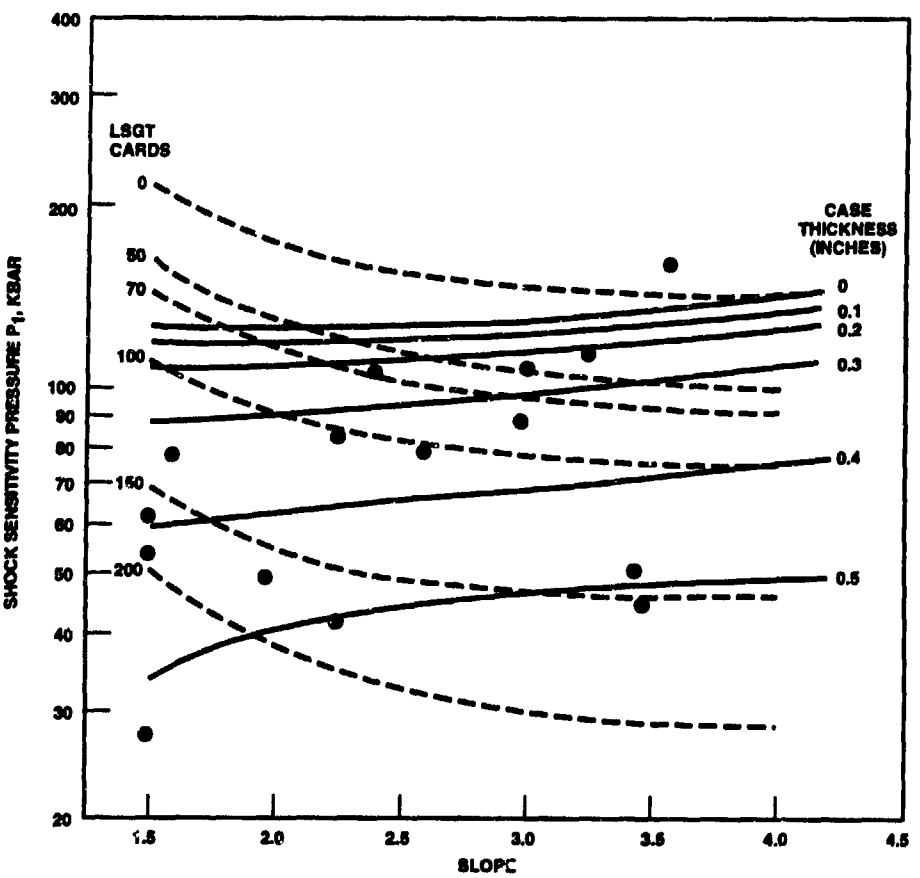

FIGURE 9. Shock Sensitivity Plane From Figure 6 Showing the Threshold Curves for Steel-Cased Explosive. The figure also includes contours of results for the large-scale gap test (LSGT).

In Figure 9, every explosive that lies on the 100-card contour, for example, will have a LSGT result of 100 cards. The most important fact that one can deduce from Figure 9 is that the LSGT contour lines are not parallel to the Golden Fragment threshold lines. This means that the LSGT is not a very good indicator of whether a particular explosive will pass the Golden Fragment test. For example, one might have a warhead with a case thickness of 0.3 inch and an explosive with a LSGT result of 70 cards. The 70-card line intersects the 0.3-inch case thickness line at a slope of about 2.9. This means that all of those explosives that have 70-card LSGT results will detonate if they also have a Pop plot slope greater than 2.9. Conversely, if the Pop plot slope is less than 2.9, the Golden Fragment test will not produce a prompt detonation.

EFFECTS OF A CASE LINER ON THE DETONATION THRESHOLD

Most cased munitions also have a liner between the case and the explosive. Calculations were performed to investigate the effect of the liner on the threshold shock sensitivity of the explosive. It has already been shown that the case thickness has a large effect on the threshold if the case is thicker than the fragment radius. The addition of a liner is expected to effectively add to the thickness. It remains in question whether the different equation of state of the liner material will make a difference.

The shock Hugoniot for two liner materials that have been used in warheads was obtained from Reference 5. For Sylgard with a density of 1.332 g/cm^3, the shock Hugoniot is

$$U_s = 0.10 + 2.46 \cdot U_p$$

and, for asphalt loaded with ammonium oxylate with a density of 1.038 g/cm^3, it is

$$U_s = 0.17 + 2.0 \cdot U_p$$

Calculations of the Golden Fragment test have been performed assuming that the entire case was composed of liner material. The threshold shock sensitivity pressure results for a Sylgard and asphalt are shown in Figure 10 for a Pop plot slope of 2.5. For comparison, the threshold curve for steel is included. There is a much larger difference in Figure 10 between the liner materials and steel than was shown in Figure 5 for steel and the rest of the case materials. The two liner materials behave similarly in Figure 10 when used as cases, so it is expected that they will yield similar behavior when used as liners.

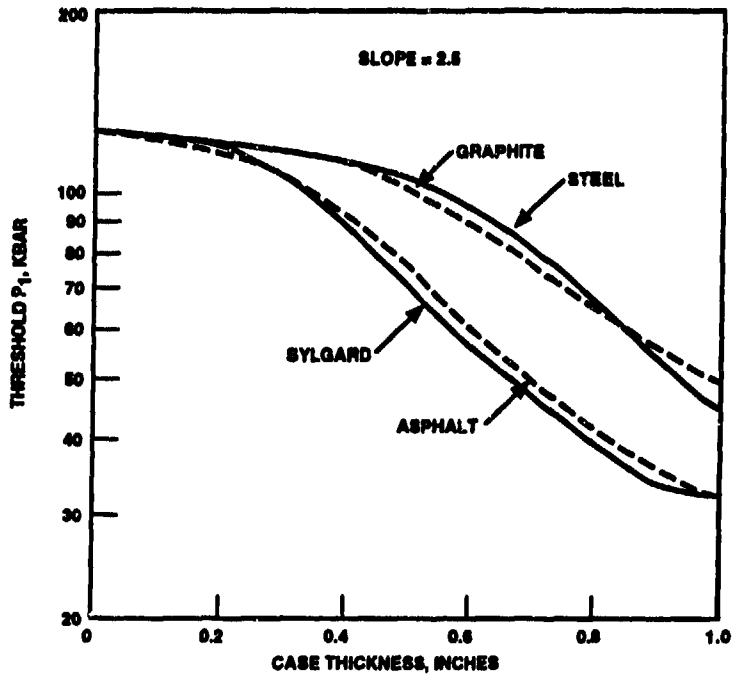

FIGURE 10. Threshold Shock Sensitivity Pressure, P_1, as a Function of Case Thickness. The figure compares results for the two liner materials, Sylgard and asphalt, with two case materials, steel and graphite.

A series of calculations was performed to show the effect of the two liner materials when used with two case materials, steel and graphite. For a steel case, the threshold shock sensitivity is plotted in Figures 11, 12, and 13 for Pop plot slopes of 1.5, 2.5, and 3.5, respectively. The results for a graphite case are similarly shown in Figures 14, 15, and 16. The threshold shock sensitivities, P_1, are plotted as a function of the steel or graphite dimensionless case thickness.

In Figure 12, the upper curve is the threshold P_1 result for a plane steel case plotted as a function of case thickness. This curve was taken from Figure 4. The remaining curves in Figure 12 represent case/liner combinations. The lowest pair of curves represent lined steel cases with a total thickness of 0.4 inch. Since the abscissa is the steel case thickness, the liner thickness is 0.4 inch at the left hand side of the graph where the two curves intersect the ordinate. At the other end, these two curves intersect the steel case curve at a case thickness of 0.8 inch; at this point, the liner thickness is zero. Curves for total case/liner thicknesses of 0.4, 0.3, and 0.2 inch are shown in each of the subsequent figures.

As noted in connection with the results for unlined cases, the Pop plot slope does not affect the threshold shock sensitivity very much, and there is no significant difference between the two liner materials, Sylgard and asphalt. However, a large difference exists in the results of lined graphite and lined steel cases. This can be seen, for example, by comparing Figure 11 with Figure 14. The difference is surprising, considering that the results in Figure 10 for the unlined steel and graphite cases are so similar.

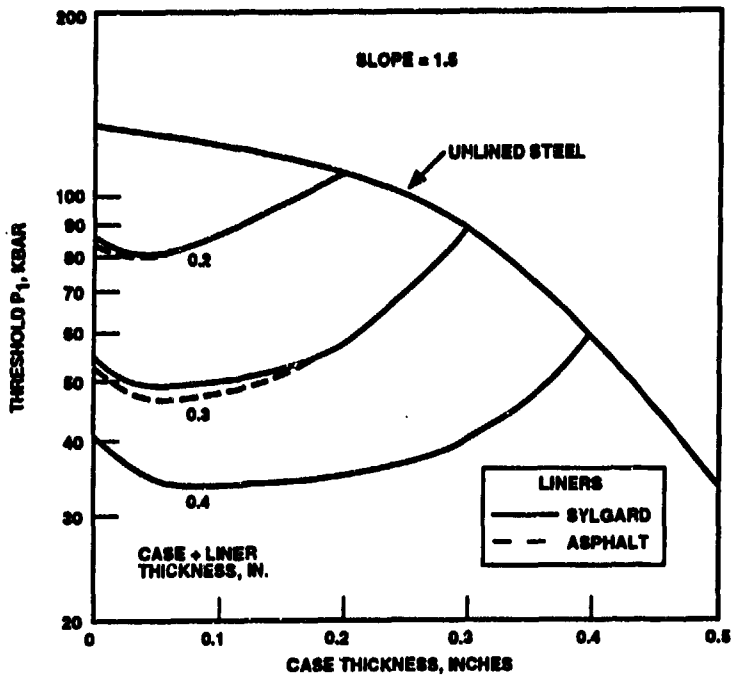

FIGURE 11. Threshold Shock Sensitivity Pressure, P_1, for Lined Munitions as a Function of the Steel Case Thickness for Slope Parameter S = 1.5. Thresholds for total case/liner thicknesses of 0.2, 0.3, and 0.4 inch are shown for Sylgard and asphalt liners.

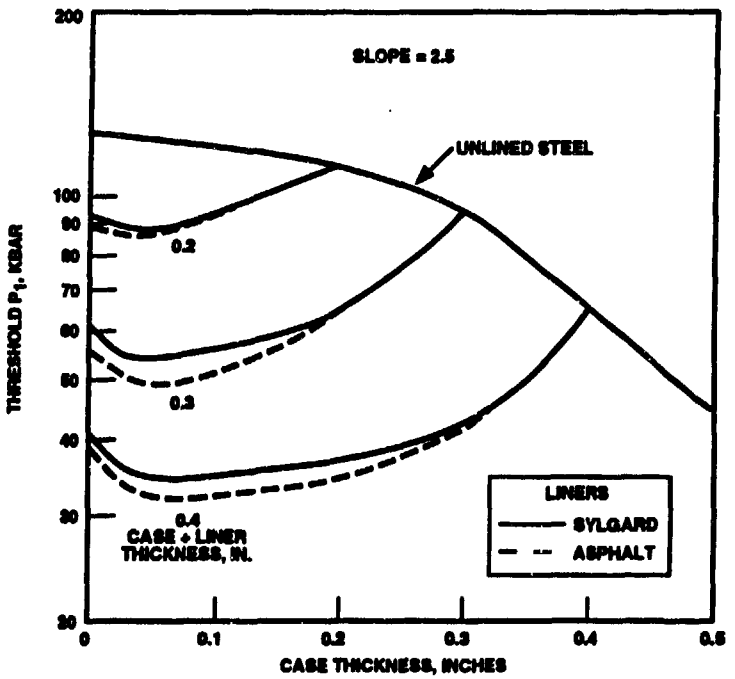

FIGURE 12. Threshold Shock Sensitivity Pressure, P_1, for Lined Munitions as a Function of the Steel Case Thickness for Slope Parameter S = 2.5. Thresholds for total case/liner thicknesses of 0.2, 0.3, and 0.4 inch are shown for Sylgard and asphalt liners.

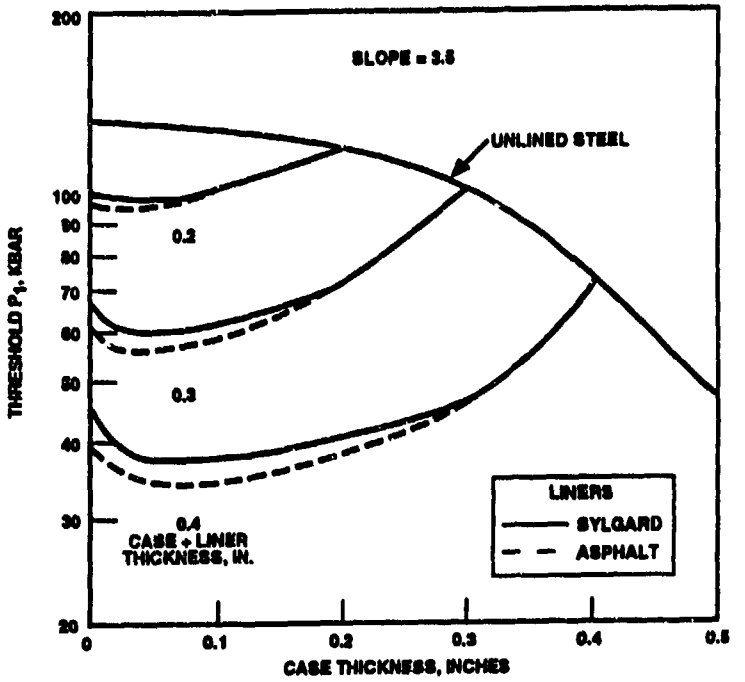

FIGURE 13. Threshold Shock Sensitivity Pressure, P_1, for Lined Munitions as a Function of the Steel Case Thickness for Slope Parameter S = 3.5. Thresholds for total case/liner thicknesses of 0.2, 0.3, and 0.4 inch are shown for Sylgard and asphalt liners.

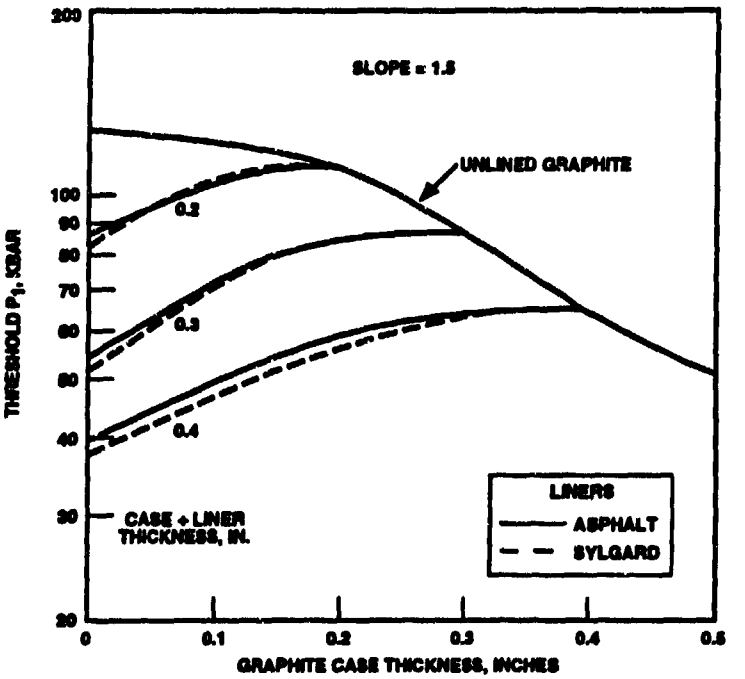

FIGURE 14. Threshold Shock Sensitivity Pressure, P_1, for Lined Munitions as a Function of the Graphite Case Thickness for Slope Parameter S = 1.5. Thresholds for total case/liner thicknesses of 0.2, 0.3, and 0.4 inch are shown for Sylgard and asphalt liners.

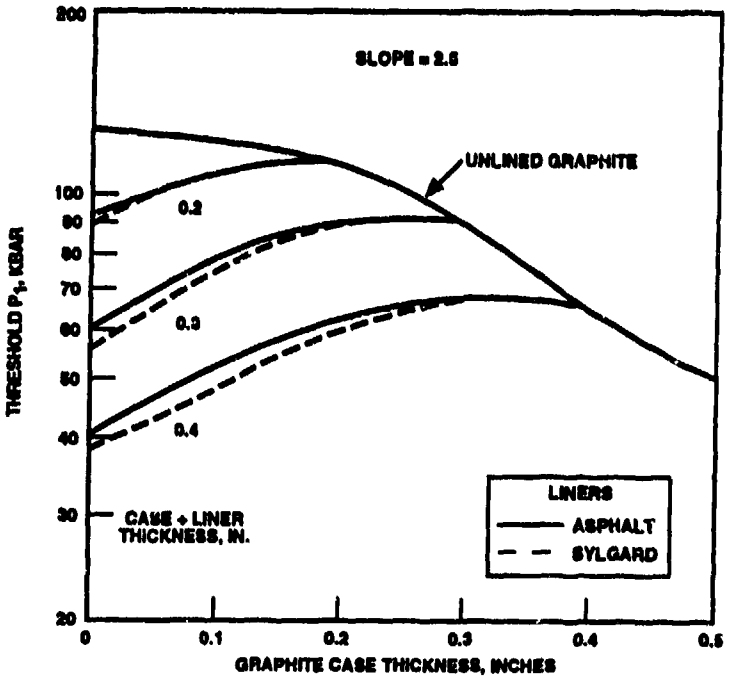

FIGURE 15. Threshold Shock Sensitivity Pressure, P_1, for Lined Munitions as a Function of the Graphite Case Thickness for Slope Parameter S = 2.5. Thresholds for total case/liner thicknesses of 0.2, 0.3, and 0.4 inch are shown for Sylgard and asphalt liners.

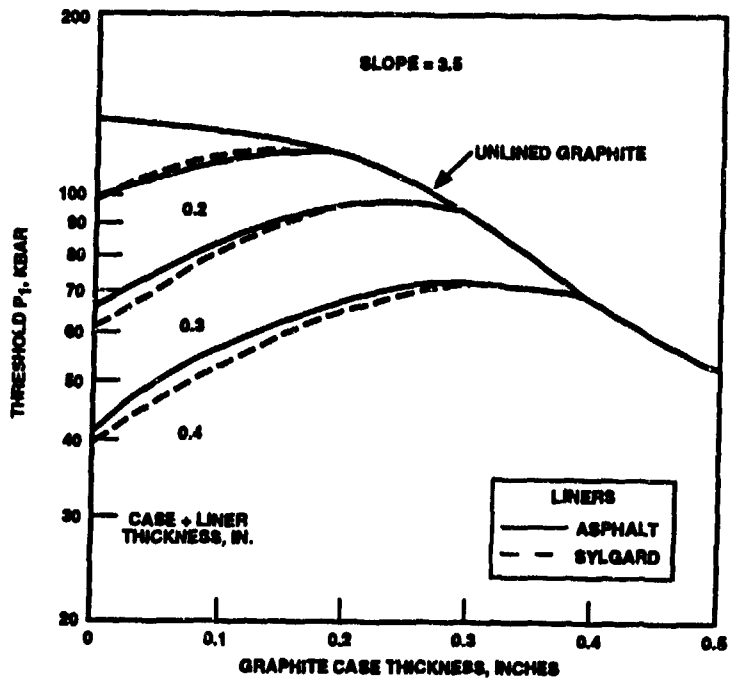

FIGURE 16. Threshold Shock Sensitivity Pressure, P_1, for Lined Munitions as a Function of the Graphite Case Thickness for Slope Parameter S = 3.5. Thresholds for total case/liner thicknesses of 0.2, 0.3, and 0.4 inch are shown for Sylgard and asphalt liners.

EXAMPLE OF CASE DESIGN TO SURVIVE FRAGMENT IMPACT

To illustrate the theory, several examples are given. First, suppose there are three explosives under consideration for a warhead, PBXN-109, PBXN-107, and PBXC-129(Q). Case material candidates are steel and titanium. The first step is to find the threshold case thickness for an unlined warhead that would prevent detonation during the fragment impact test. From Figure 3, PBXN-109 has a shock sensitivity pressure $P_1 = 64$ kbar. It has a Pop plot slope of 1.5, so that Figure 4 can be used directly to get the threshold case thickness. The threshold curve for the steel case crosses the $P_1 = 64$ kbar level when the case thickness is 0.39 inch. If the steel case is thinner than 0.39 inch, then the fragment impact test is predicted to result in detonation. For a titanium case, Figure 4 gives a threshold case thickness of 0.47 inch. Similarly, from Figure 3, the Pop plot slope for PBXC-129(Q) is 3.5, so that Figure 6 can be used directly. It follows that the threshold case thickness for steel-cased PBXC-129(Q) is 0.43 inch and for a titanium case is 0.47 inch.

From Figure 3, the Pop plot slope of PBXN-107 is about 2.0. One can get the threshold P_1 for this slope by interpolating the data for slopes 1.5 and 2.5 in Table B-1 of Appendix B for the unlined steel case. For the titanium case, the data in Table B-3 is interpolated. The resulting threshold values are shown in Table 1 and plotted in Figure 17.

TABLE 1. Threshold Shock Sensitivity for Steel- and Titanium-Cased Explosive With Slope of 2.5.

Case Thickness, in	Threshold P_1, kbar	
	Steel	Titanium
0.00	129.0	129.0
0.05	124.0	132.0
0.10	120.0	131.0
0.15	116.0	128.0
0.20	110.0	124.0
0.25	102.0	118.0
0.30	90.7	110.0
0.35	76.5	98.0
0.40	62.5	82.7
0.45	52.0	69.2
0.50	43.7	58.5

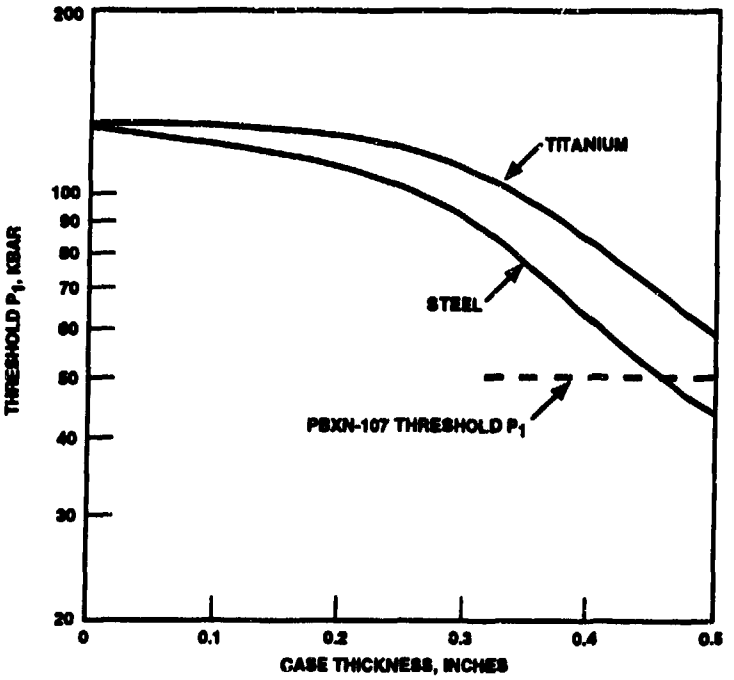

FIGURE 17. Threshold Shock Sensitivity Pressure, P_1, as a Function of Case Thickness for a Slope Parameter of S = 2.0. Curves for steel and titanium cases are shown. The value of P_1 = 49 kbar for PBXN-107 is indicated.

From Figure 17, the threshold steel case thickness is 0.46 inch. The intersection of the titanium curve with the PBXN-107 threshold shock sensitivity lies off the figure, but it should be about 0.54 inch. The resulting threshold case thicknesses for the example are summarized in Table 2.

TABLE 2. Threshold Steel and Titanium Case Thicknesses for the Example Explosives, PBXN-109, PBXN-107, and PBXC-129(Q).

Explosive	Steel Thickness, in	Titanium Thickness, in
PBXN-109	0.39	0.47
PBXN-107	0.46	0.54
PBXC-129(Q)	0.43	0.47

If the warhead has a liner, Figures 11 through 13 show that the threshold shock sensitivity for the combined steel case and asphalt or Sylgard liner is always less than the threshold for the same thickness of steel. This is also probably true for titanium cases with liners, since the shock impedance of titanium lies between that of steel and graphite. One can then regard the case thicknesses in Table 2 as conservative estimates for the threshold value of the combined case and liner thickness.

The threshold shock sensitivity for steel cases lined with asphalt or Sylgard has already been worked out, so one can compare the effect of different liner thicknesses on the required case thickness. Figure 18 repeats portions of Figure 11 for an asphalt-lined, steel-cased explosive with a slope parameter of 1.5. The plots were drawn using the calculated data from Table B-8 in Appendix B. Two additional curves that give threshold P_1 for total case/liner thicknesses of 0.25 and 0.35 inch have been added. The shock sensitivity pressure $P_1 = 64$ kbar for PBXN-109 has been added as a horizontal line. The various critical thicknesses can be obtained where the PBXN-109 line intersects the threshold curves. Table 3 summarizes the results.

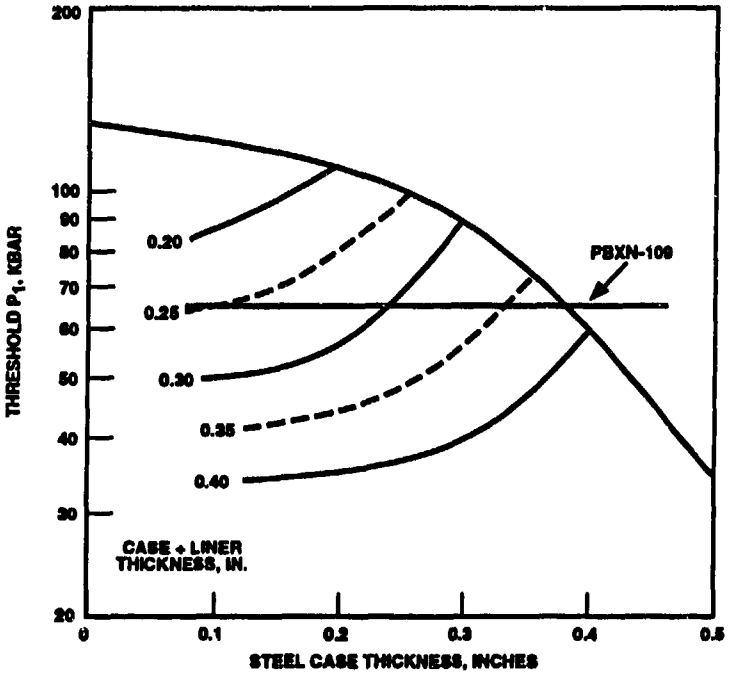

FIGURE 18. Threshold Shock Sensitivity Values for a Steel Case Lined With Asphalt as a Function of the Case Thickness for Slope Parameter S = 1.5. The solid curves were taken from Figure 11 (Table B-6). The broken curves are estimates.

TABLE 3. Threshold Thickness for Steel-Cased PBXN-109 Lined With Asphalt. The thicknesses are given in inches.

Total	Case	Liner
0.38	0.38	0.00
0.35	0.33	0.02
0.30	0.24	0.06
0.25	0.10	0.15

The liner thickness required for detonation threshold is plotted in Figure 19 as a function of case thickness. The plot shows the combination of asphalt liner and steel case thickness that will pass the fragment impact test with PBXN-109.

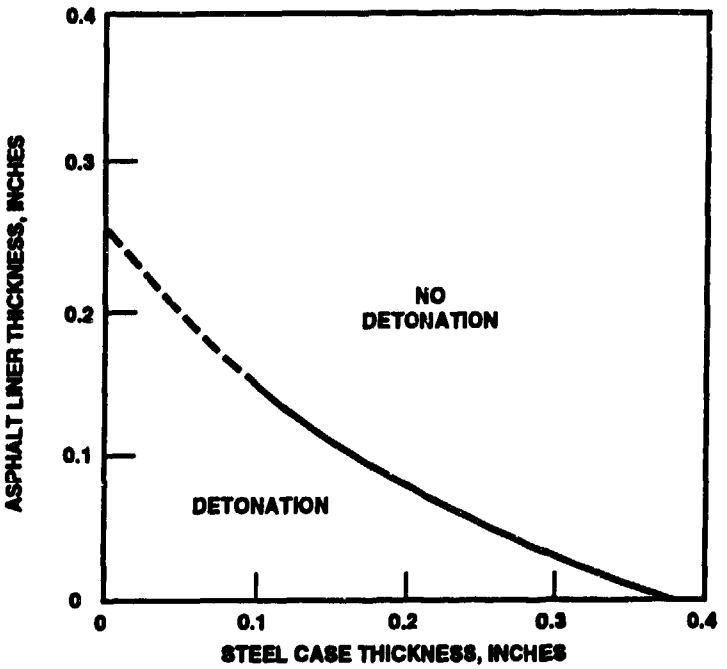

FIGURE 19. Combinations of Steel Case Thickness and Asphalt Liner Thickness That Will Prevent Prompt Detonation of PBXN-109 in the Golden Fragment Test.

EXAMPLE OF EXPLOSIVE SELECTION

As a second example, suppose that an insensitive explosive is desired as a replacement in an existing warhead. The case material and thickness are likely to be fixed. The liner material and thickness may have to be adjusted for compatibility with the replacement explosive. For definiteness, suppose the case is 0.25-inch-thick steel and the liner material is asphalt.

The best way to make the explosive selection is to use the shock sensitivity plane. The threshold values of the shock sensitivity plane for the steel case/asphalt liner system can be obtained from Figures 11, 12, and 13 for values of the slope parameter of 1.5, 2.5, and 3.5, respectively. The corresponding tables in Appendix B can also be used. In Figure 11, for example, draw a vertical line at a case thickness of 0.25 inch. The values of P_1 as a function of total case and liner thickness can then be attained. The results are tabulated in Table 4.

TABLE 4. Threshold Shock Sensitivity Pressure for a 0.25-Inch-Thick Steel Case as a Function of Asphalt Liner Thickness.

Case + Liner Thickness, in	Liner Thickness, in	P_1 (kbar)		
		Slope = 1.5	Slope = 2.5	Slope = 3.5
0.25	0.00	99.2	104.7	113.2
0.30	0.05	67.7	76.2	85.2
0.40	0.15	36.7	39.2	43.2

The thresholds are plotted on the shock sensitivity plane in Figure 20. The points denote explosives which were included in Figure 3. The labels for the explosive points were left off in the interest of clarity. As usual, in order to pass the test without a prompt detonation, the explosive must lie above the appropriate threshold curve. One can see from Figure 20 that the liner can have a significant effect on the range of explosives which can pass the fragment impact test. With no liner, none of the most commonly used main charge explosives will pass. With the 0.15-inch asphalt liner, any of the common main charge explosives will pass. Part of the reason for this is that the case itself is 0.25 inch thick. The combination of case and liner is at least as effective as the same total thickness of case material. As can be seen in Figure 4, for example, after 0.25 inch, the effectiveness of the case starts to increase dramatically.

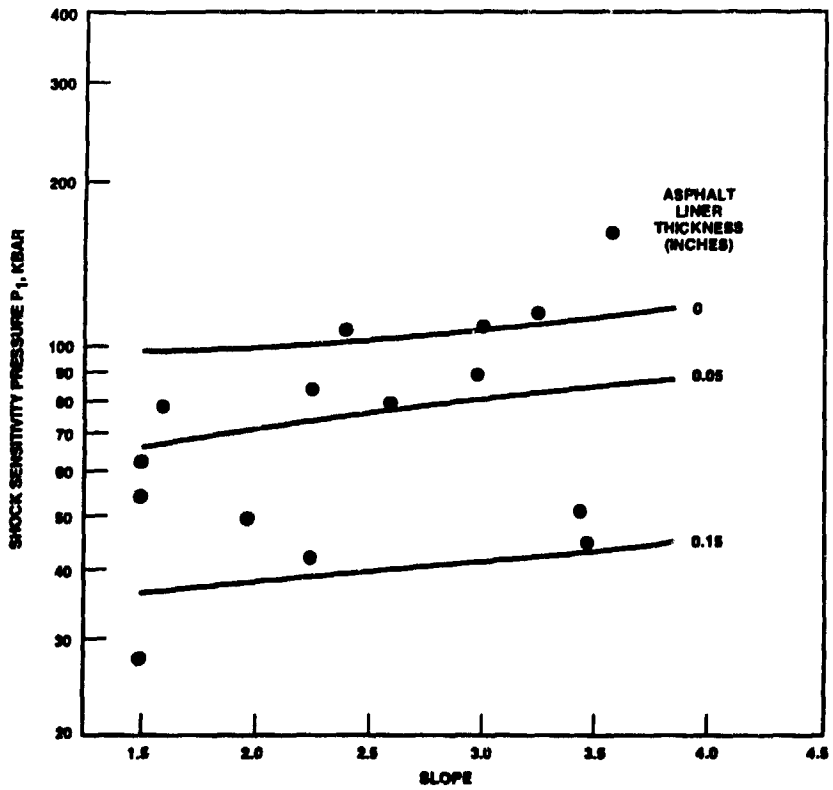

FIGURE 20. Effect of the Asphalt Liner Thickness on the Response of an Explosive Cased With a 0.25-Inch-Thick Steel Case. Points represent shock sensitivity of explosives as shown in Figure 3.

To use the shock sensitivity plane technique, it is convenient to make a separate plot of the plane with all of the explosive points on it and a separate plot of the threshold curves drawn to the same scale. The two plots then are overlayed to see the relationship of the explosive points to the threshold curves. A third plot can also be constructed showing the large-scale card test contours, as was done in Figure 9. This can also be useful if there is no wedge test data available for the explosive of interest.

SUMMARY

Criteria for choosing an energetic material that will pass the Golden Fragment test in generic ordnance configurations have been derived. The tool used for generating the criteria was the SMERF computer code. The effect of a case liner on the detonation threshold of an explosive, and examples of case design that can survive fragment impact and explosive selection are discussed.

REFERENCES

1. Naval Sea Systems Command. *Insensitive Munition Program Planning and Execution*. Washington, D. C., NAVSEA Instruction 8010.5.

2. Naval Weapons Center. *Evaluation of Forest Fire Burn Model of Reaction Kinetic of Heterogeneous Explosives*, by E. A. Lundstrom. China Lake, Calif., NWC, May 1988. (NWC TP 6898, publication UNCLASSIFIED.)

3. E. A. Lundstrom. "A New Approach to Shock Sensitivity Testing of Energetic Materials," in the Proceedings of the 1989 JANNAF Propulsion Systems Hazards Subcommittee Meeting, CPIA Publication 509, February 1989.

4. E. A. Lundstrom. "Shock Sensitivity Testing and Analysis for a Minimum-Smoke Propellant," in the Proceedings of the 1991 JANNAF Propulsion Systems Hazards Subcommittee Meeting, March 1991.

5. U.S. Army Missile Command. *A Study of Shock Mitigation Using Numerical Simulations of Propellant Case Designs*, by D. Littlefield. Redstone Arsenal, MICOM, September 1992. (Technical Report CR-RD-PR-92-3, publication UNCLASSIFIED.)

6. M. D. Cook, P. J. Haskins, and H. R. James. "Projectile Impact Initiation of Explosive Charges," in the Proceedings of the Ninth Symposium (International) on Detonation, Office of the Chief of Naval Research, OCNR 113291-7, September 1989.

7. E. A. Lundstrom. "A Hot Spot Variation of the Forest Fire Burn Model for Condensed Heterogeneous Explosives," in the Proceedings of the 22nd International Conference of ICT, Fraunhoffer-Institut for Chemische Technologie, July 1991.

8. A. Lindfors, Naval Air Warfare Center, China Lake, California, Private Communication.

Appendix A
WEDGE TEST DATA

This appendix contains wedge test data in the form of Pop plot constants, P_1 and slope, shown in the shock sensitivity plane plots in this report. It also contains the linear U_s-U_p fits of the shock Hugoniot data that were taken in the same wedge tests. The coefficients in the Hugoniot equation are defined by

$$U_s = a + b \cdot U_p$$

where U_s is the shock velocity and U_p is the particle velocity.

TABLE A-1. Wedge Test Results for Selected Explosives.

Explosive	Density, g/cm^3	a, cm/μs	b	P_1, kbar	Slope	Reference
AFX-1100	1.53	0.206	2.16	84.4	2.216	2
Comp B	1.715	0.231	2.50	54.0	1.501	9
Destex	1.69	0.2998	1.481	79.4	2.63	1
PBXN-3	1.70	0.195	3.37	44	3.42	5
PBXN-103	1.89	0.267	1.78	90	2.941	10
PBXN-107	1.626	0.243	2.08	48.4	1.97	6
PBXN-109	1.66	0.175	2.78	64	1.32	3
PBXN-110	1.68	0.247	1.27	79.1	1.6	7
PBXC-129(Q)	1.71	0.233	3.04	47.6	3.45	4
PBXW-108E	1.565	0.163	2.46	46	2.24	11
PBX-9404	1.84	0.2494	2.093	28.8	1.538	1
PBX-9502	1.894	0.24	2.5	113.5	2.917	9
Tritonal	1.73	0.2313	2.769	105	2.41	8
TNT	1.654	0.2109	2.337	120	3.125	1
X-0219	1.914	0.240	2.05	161	3.54	9

REFERENCES
(For Wedge Test Data.)

1. T. Gibbs and A. Popolato. *LASL Explosive Property Data*. University of California Press, 1980.

2. J. Dallman. *Characterization of Air Force Explosive AFX-1100 II*, LA-OR 88-4221.

3. Naval Weapons Center. *Explosives Advanced Development Program, Safety and Vulnerability Evaluation of PBXC-117E and PBXW-109E (U)*, by M. Wagenhals and W. Smith. China Lake, Calif., NWC, December 1982. (NWC TP 6388, publication CONFIDENTIAL.)

4. Naval Weapons Center. *Wedge Test Results for PBXC-129*, by A. Lindfors. China Lake, Calif., NWC, 1991. (NWC Reg. Memo 3894/033, document UNCLASSIFIED.)

5. Los Alamos National Laboratory. *Wedge Tests of PBXN-3*, by I Akst. Los Alamos, NM, LANL, 1987. (LANL Report No. M-8-87-1, publication UNCLASSIFIED.)

6. Naval Weapons Center. *Wedge Test Results for PBXN-107 Type II*, by A. Lindfors and F. Sandstrom. China Lake, Calif., NWC, 1990. (NWC TM 6792, publication UNCLASSIFIED.)

7. ----------. Shock Initiation of PBXW-113 Using the Wedge Technique, by T. Schilling and S. Martin. China Lake, Calif., NWC. (NWC TP 6961, publication UNCLASSIFIED.)

8. B. Craig, private communication.

9. C. Mader. *Numerical Modeling of Detonations*. University of California Press, 1979.

10. J. Dahlman. "Wedge Tests of PBXN-103 Explosive," Memo M-9, 13 April 1988.

11. Naval Weapons Center. *Explosives Advanced Development Program Safety and Vulnerability Evaluation of PBXAF-108E and PBXW-108E (U)*, by S. Christian, M. Wagenhals, G. Green, and T. Joyner. China Lake, Calif., NWC, May 1986. (NWC TP 6484, publication CONFIDENTIAL.)

Appendix B
THRESHOLD SHOCK SENSITIVITY DATA

This appendix contains the threshold shock sensitivity data for a variety of cases.

TABLE B-1. Threshold Shock Sensitivity for an Unlined Steel Case.

Thickness, in	P_1, kbar		
	Slope = 1.5	Slope = 2.5	Slope = 3.5
0.00	129.7	128.2	134.2
0.05	124.2	123.7	130.7
0.10	120.0	120.7	127.7
0.15	114.7	117.2	124.2
0.20	107.5	111.7	119.7
0.25	99.2	104.7	113.2
0.30	87.2	94.2	103.2
0.35	72.7	80.2	88.7
0.40	59.7	65.2	72.2
0.45	50.2	53.7	58.2
0.50	43.2	44.2	47.7

TABLE B-2. Threshold Shock Sensitivity for an Unlined Aluminum Case.

Thickness, in	P_1, kbar		
	Slope = 1.5	Slope = 2.5	Slope = 3.5
0.00	129.7	128.2	134.2
0.05	126.7	125.7	132.2
0.10	125.7	126.5	131.7
0.15	121.7	122.2	129.2
0.20	116.2	117.7	125.7
0.25	108.2	111.7	120.2
0.30	97.7	103.2	111.7
0.35	82.7	89.7	98.5
0.40	68.2	74.2	81.7
0.45	57.7	61.7	67.7
0.50	50.2	52.2	56.7

TABLE B-3. Threshold Shock Sensitivity for an Unlined Titanium Case.

Thickness, in	P_1, kbar		
	Slope = 1.5	Slope = 2.5	Slope = 3.5
0.00	129.7	128.2	134.2
0.05	133.7	130.7	137.7
0.10	131.7	130.2	136.7
0.15	128.2	127.7	134.7
0.20	123.7	124.0	131.7
0.25	116.7	118.7	126.5
0.30	107.7	111.7	119.7
0.35	95.2	100.7	109.2
0.40	79.7	85.7	93.2
0.45	67.2	71.2	77.7
0.50	57.2	59.7	64.7

TABLE B-4. Threshold Shock Sensitivity for an Unlined Graphite Case.

Thickness, in	P_1, kbar		
	Slope = 1.5	Slope = 2.5	Slope = 3.5
0.00	129.7	128.2	134.2
0.05	125.5	124.2	131.2
0.10	121.7	121.7	128.7
0.15	118.2	118.7	125.7
0.20	110.7	112.2	118.7
0.25	99.2	101.3	107.7
0.30	85.7	88.5	93.5
0.35	74.2	75.5	80.2
0.40	64.7	65.2	68.7
0.45	56.7	56.2	58.7
0.50	50.5	48.7	50.2

TABLE B-5. Threshold Shock Sensitivity for an Unlined Asphalt Case.

Thickness, in	P_1, kbar		
	Slope = 1.5	Slope = 2.5	Slope = 3.5
0.00	129.7	128.2	134.2
0.05	125.2	124.7	131.7
0.10	114.2	116.2	123.7
0.15	101.2	105.7	114.2
0.20	86.0	92.2	101.0
0.25	68.7	74.7	82.2
0.30	56.2	60.2	66.2
0.35	47.2	49.7	54.2
0.40	41.0	41.5	45.2
0.45	41.2	35.7	38.2
0.50	42.5	32.7	32.7

TABLE B-6. Threshold Shock Sensitivity for an Unlined Sylgard Case.

Thickness, in	P_1, kbar		
	Slope = 1.5	Slope = 2.5	Slope = 3.5
0.00	129.7	128.2	134.2
0.05	125.7	124.7	132.2
0.10	116.2	120.8	125.7
0.15	102.2	106.7	114.7
0.20	82.5	88.5	96.6
0.25	64.7	69.7	76.2
0.30	52.7	56.2	61.2
0.35	44.7	46.2	49.7
0.40	40.7	39.2	41.7
0.45	43.5	33.7	35.7
0.50	43.5	32.7	32.7

TABLE B-7. Threshold Shock Sensitivity for a Steel Case Lined With Asphalt as a Function of Case Thickness, T_C, and Liner Thickness, T_L.

$T_C + T_L$, in	T_L, in	P_1, kbar		
		Slope = 1.5	Slope = 2.5	Slope = 3.5
0.2	0.000	107.5	111.7	119.7
	0.050	96.2	102.7	111.2
	0.100	84.7	92.2	101.2
	0.125	82.2	90.2	99.7
	0.150	80.7	88.7	97.7
	0.175	80.7	88.2	97.2
	0.200	86.0	92.5	101.0
0.3	0.000	87.2	94.2	103.2
	0.050	67.7	76.2	85.2
	0.100	55.7	63.7	71.7
	0.150	51.7	58.7	65.7
	0.200	49.7	55.2	62.2
	0.225	49.7	54.7	60.7
	0.250	48.7	53.7	59.7
	0.275	49.7	54.7	60.2
	0.300	56.2	60.2	66.2
0.4	0.000	59.7	65.2	72.2
	0.050	45.5	49.2	54.7
	0.100	38.7	42.2	46.7
	0.150	36.7	39.2	43.2
	0.200	35.0	37.2	40.7
	0.250	33.7	35.4	38.6
	0.300	33.2	34.8	37.6
	0.325	33.7	34.7	37.5
	0.350	35.2	34.7	37.5
	0.375	36.2	36.2	39.2
	0.400	40.2	41.0	45.2

TABLE B-8. Threshold Shock Sensitivity for a Steel Case Lined With Sylgard as a Function of Case Thickness, T_C, and Liner Thickness, T_L.

$T_C + T_L$, in	T_L, in	P_1, kbar		
		Slope = 1.5	Slope = 2.5	Slope = 3.5
0.2	0.000	107.5	111.7	119.7
	0.050	97.2	103.2	111.7
	0.100	86.7	94.2	103.7
	0.125	82.7	90.7	99.7
	0.150	79.7	87.7	96.7
	0.175	78.2	85.7	93.7
	0.200	82.5	88.5	96.5
0.3	0.000	87.2	94.2	103.2
	0.050	68.7	77.2	86.2
	0.100	56.2	64.2	72.7
	0.150	50.2	56.2	63.2
	0.200	47.2	52.2	57.7
	0.225	46.7	50.7	56.2
	0.250	45.7	50.2	55.2
	0.275	47.2	50.2	55.2
	0.300	52.7	56.2	61.2
0.4	0.000	59.7	65.2	72.2
	0.050	46.2	51.2	55.7
	0.100	38.7	42.2	46.7
	0.150	35.2	37.7	41.7
	0.200	33.2	34.7	38.2
	0.250	–	33.2	33.7
	0.300	–	32.2	34.7
	0.325	–	32.2	34.7
	0.350	39.2	32.2	34.2
	0.375	–	34.2	36.2
	0.400	40.7	33.7	35.7

TABLE B-9. Threshold Shock Sensitivity for a Graphite Case Lined With Asphalt as a Function of Case Thickness, T_C, and Liner Thickness, T_L.

$T_C + T_L$, in	T_L, in	P_1, kbar		
		Slope = 1.5	Slope = 2.5	Slope = 3.5
0.2	0.000	110.7	112.2	118.7
	0.050	108.2	110.7	118.7
	0.100	104.2	108.2	115.7
	0.125	100.2	104.7	112.7
	0.150	95.7	100.7	109.2
	0.175	89.7	96.2	104.7
	0.200	86.0	92.2	101.0
0.3	0.000	85.7	88.5	93.5
	0.050	86.2	90.7	97.7
	0.100	85.2	90.7	97.7
	0.150	79.7	85.7	92.2
	0.200	72.2	75.7	84.7
	0.225	67.2	73.2	80.2
	0.250	62.7	68.2	75.2
	0.275	57.7	63.2	69.7
	0.300	56.2	60.2	56.2
0.4	0.000	65.0	65.2	68.7
	0.050	64.2	67.2	71.7
	0.100	63.7	67.2	72.7
	0.150	61.7	65.2	70.7
	0.200	58.7	62.2	67.2
	0.250	54.7	57.7	62.7
	0.300	49.2	52.2	56.7
	0.325	46.2	48.7	53.2
	0.350	43.2	45.7	49.2
	0.375	41.2	42.7	46.2
	0.400	45.2	41.7	40.7

TABLE B-10. Threshold Shock Sensitivity for a Graphite Case Lined With Sylgard as a Function of Case Thickness, T_C, and Liner Thickness, T_L.

$T_C + T_L$, in	T_L, in	P_1, kbar		
		Slope = 1.5	Slope = 2.5	Slope = 3.5
0.2	0.000	111.0	112.2	118.7
	0.050	111.2	108.7	119.7
	0.100	105.7	108.7	116.7
	0.125	102.2	106.7	114.7
	0.150	97.2	102.2	116.7
	0.175	89.7	95.7	103.7
	0.200	82.5	88.5	96.5
0.3	0.000	85.7	88.5	93.5
	0.050	86.7	90.7	97.2
	0.100	84.2	89.2	96.7
	0.150	77.2	82.7	89.2
	0.200	70.2	75.7	82.2
	0.225	65.2	70.7	77.2
	0.250	60.2	65.2	71.2
	0.275	55.2	59.2	64.7
	0.300	52.7	56.2	61.2
0.4	0.000	64.7	65.2	68.7
	0.050	64.7	67.2	72.2
	0.100	63.2	67.2	72.7
	0.150	59.7	63.2	68.2
	0.200	55.7	58.7	63.7
	0.250	51.2	54.2	58.7
	0.300	46.8	49.2	53.2
	0.325	43.8	45.9	49.7
	0.350	41.1	42.7	45.7
	0.375	39.1	39.7	42.7
	0.400	39.2	41.7	40.7

Appendix C
THRESHOLD SHOCK SENSITIVITY FOR LSGT

This appendix presents the numerical values of the threshold shock sensitivity for the large-scale gap test.

TABLE C-1. Threshold Shock Sensitivity Pressure for Large-Scale Gap Test.

Gap, cards	P_1, kbar					
	S = 1.5	S = 2.0	S = 2.5	S = 3.0	S = 3.5	S = 4.0
0	216.5	173.4	155.2	147.6	142.9	142.2
50	163.2	128.8	114.3	106.8	101.6	98.4
70	143.3	115.7	103.5	97.6	94.5	91.5
100	111.1	90.3	82.2	78.2	75.7	74.7
150	68.5	54.0	49.2	46.8	46.1	45.9
200	50.4	37.9	32.8	30.1	28.9	28.1

INITIAL DISTRIBUTION

22 Naval Air Systems Command, Arlington
- AIR-09E1 (1)
- AIR-09F (1)
- AIR-516 (1)
- AIR-516C (1)
- AIR-516C1, Barber (1)
- AIR-540 (1)
- AIR-540TF, Magnelli (1)
- AIR-5401 (1)
- AIR-5402 (1)
- AIR-5403 (1)
- AIR-5404 (1)
- PMA-201 (5)
- PMA-242 (1)
- PMA-253 (1)
- PMA-258 (1)
- PMA-259 (1)
- PMA-268 (1)
- PMA-280 (1)

3 Chief of Naval Operations
- OP-410 (1)
- OP-411 (1)
- OP-982E4 (1)

1 Chief of Naval Research, Arlington (ONR-410)

7 Naval Sea Systems Command, Arlington
- SEA-665, E. Kratcvil (1)
- SEA-6652, P. Wright (1)
- SEA-91 (1)
- SEA-91WM, Dr. R. Bowen (4)

1 Naval Air Warfare Center Air Division, Lakehurst (Code 53, Systems Engineering and Standardization Department)

1 Naval Air Warfare Center Weapons Division, Point Mugu (Code PO3512, Morcos)

1 Naval Air Warfare Center Weapons Division Detachment, Kirtland Air Force Base (Code 22, J. Stickney)

3 Naval Construction Battalion Center, Port Hueneme
- Code L51
  - W. Armstrong (1)
  - W. Kennan (1)
  - J. Tancreto (1)

3 Naval Explosive Ordnance Disposal Technology Center, Indian Head
- Code 044, R. Poe (1)
- Code 20 (1)
- Code 60 (1)

11 Naval Surface Warfare Center Division, Crane
- Code 4021, D. Wildridge (1)
- Code 4025, L. Wilson (1)
- Code 4041
  - Cooper (1)
  - Papp (1)
  - Whorrall (1)
- Code 4071
  - Broxton (1)
  - Lohkamp (1)
- Code 50 (1)
- Code 5011 (1)
- Code 50223 (1)
- Technical Library (1)

16 Naval Surface Warfare Center, Dahlgren Division Detachment White Oak, Silver Spring
- R04, Dickinson (1)
- R10B, Haiss (1)
- R10H, Swiskda (1)
- R101, Roslund (1)
- R12, Spahn (1)
- R13, P. Miller (1)
- R16
  - Baudler (1)
  - Mensi (1)
- G08
  - R. Kavetsky (1)
  - E. P. Johnson (1)
- G81, O. Parrent (1)
- G40
  - J. Bagnall (1)
  - D. Grenier (1)
- G411, A. Munach (1)
- U32, O. Parrent (1)
- Technical Library (1)

17 Naval Surface Warfare Center Division, Dahlgren
- G06, R. Stayton
- G20, D. Brunson (1)
- G22
  - Grigsby (1)
  - Holt (1)
  - Hoye (1)
  - Swierk (1)
  - Vittoria (1)
  - Waggener (1)
  - Wilson (1)
- G31, Monolo (1)
- H11 (1)
- H12 (1)
- R15
  - D. Houchins (1)
  - J. Powell (1)
- R35, Dr. B. Smith (1)
- G. Credle (1)
- D. Dickenson (1)

4 Naval Surface Warfare Center Division, Indian Head
- Code 04, M. Hudson (1)
- Code 20 (1)
- Code 340, L. Miller (1)
- Code 8420G, Standardization Branch (1)

2 Naval Undersea Warfare Center Division, Keyport
- Code 04, K. Scott (1)
- C. Webb (1)

3 Naval Weapons Station Earle, Colts Neck (Packing, Handling, Storage and Transportability Center)
- Code 5011, Bender (1)
- Code 5014, Sova (1)
- Code 5021, Lee (1)

1 Office of Naval Technology, Arlington

3 Office of the Secretary of the Army
- DACS-SF, R. Fatz (1)
- DALO-SMA (1)
- JDPSS-SAF (1)

1 Army Armament, Munitions and Chemical Command, Picatinny Arsenal (AMCPM-AL, W. Liska)

1 Army Armament, Munitions and Chemical Command, Rock Island Arsenal(AMSMC-DSM-D, M. Johnson)

4 Army Materiel Command, Alexandria
- AMCAM-LG, R. Fahy (1)
- AMCDNR-IP (1)
- AMCSF-S (1)
- Executive Director for Explosives Safety (1)

1 Army Materiel Command, Field Safety Activity, Charlestown (AMXOS-SE, P. Yutmeyer)

11 Army Missile Command, Redstone Arsenal
- AMSMI-RD (1)
- AMSMI-RD-PR (1)
  - E. D. Dreitzler (1)
- AMSMI-RD-PR-T
  - J. Murfree, Jr. (1)
  - L. B. Thorn (1)
- AMSMI-RD-SE (1)
- AMSMI-RD-SF (1)
- AMSMI-RD-ST (1)
- AMSMI-RD-TE (1)
- AMSMI-RD-TE-F, J. Porter (1)
- AMSMI-RD-TE-S, J. Knorr (1)

3 Army Test and Evaluation Command, Aberdeen Proving Ground
- AMSTE-TA (1)
- AMSTE-TC-D, H. Egbert (1)
- AMSTE-TC-M, R. Hayes (1)

22 Army Armament Research, Development and Engineering Center, Picatinny Arsenal
- AMCPM-FZ (1)
- AMSMC-QA(D) (1)
- AMSMC-QAU(D) (1)
- AMSMC-QAR(D) (1)
- AMSMC-QAW(D) (1)
- SLCHE-AR (1)
- SMCAR-AEC-TE, E. Stewart (1)
- SMCAR-AEE, M. Mezger (1)
- SMCAR-AEE-B (1)
- SMCAR-AEE-W (1)
- SMCAR-AEF-C (1)
- SMCAR-AEM, P. Serao (1)
- SMCAR-AEP (1)
- SMCAR-AES (1)
- SMCAR-BAC-S (1)
- SMCAR-CC (1)
- SMCAR-ESW-F(R) (1)
- SMCAR-FMS-S, Saks (1)
- SMCAR-FS (1)
- SMCAR-FSM (1)
- SMCAR-SF, A. Larson (1)
- P. Lu (1)

3 Army Ballistic Research Laboratory, Aberdeen Proving Ground
- SLCBR-TB-B (1)
- SLCBR-TB-BB (1)
- SLCBR-TB-EE (1)

2 Army Combat Systems Test Agency, Aberdeen Proving Ground
  STECS-SOM
    R. Gil (1)
    R. Shipe (1)
4 Army Defense Ammunition Center and School, Savanna
  SMCAC-ES, G. Abrisz (1)
  SMCAC-ESP
    S. Blunk (1)
    J. Byrd (1)
  SMCAC-ESS, Dr. S. Kwak (1)
2 Army Engineer Waterways Experiment Station, Corps of Engineers, Vicksburg
  CEWES-SE, L. K. Davis (1)
  CEWES-SS, S. Woodson (1)
1 Army Ordnance Missile and Munitionis Center and School, Fort McClellan (ATSK-CMI-Z)
1 Army Safety Center, Fort Rucker (CSSC-PR)
1 Army Technical Center for Explosive Safety, Savanna (SMCAA-ES)
2 Army White Sands Missile Range
  STEWS-TE-N (1)
  STEWS-TE-NP (1)
1 Headquarters, Dugway Proving Ground (MT-TM-A)
2 Air Force Phillips Laboratory, Edwards Air Force Base
  C. Merrill (1)
  R. Weiss (1)
1 Air Force Phillips Laboratory, Kirtland Air Force Base (OLAC PL/NTE)
1 Air Force Safety Agency, Kirtland Air Force Base (AFSA/SEW,
  Chief Master Sergeant T. Beggs)
11 Air Force Wright Laboratories, Armament Directorate, Eglin Air Force Base
  ASC/YMEA (2)
  ASC/YQY, Janus (1)
  ASC/SEST (1)
  MSD/ENS (1)
  PMA-268, Crockett (1)
  WL/MNME
    Corley (1)
    Glenn (1)
    Dr. R. McKenney, Jr. (1)
    Parsons (1)
  WL/MNMW, Foster (1)
2 Air Force Wright Laboratories, Dynamics Directorate, Wright-Patterson Air Force Base
  WL/IGFW, W. Rieder (1)
  A. Kurtz (1)
3 Air Logistic Center, Hill Air Force Base
  ALC/MMW (1)
  ALC/MMWE (1)
  TIRRPN, 6501 Range Squadron (1)
1 Defense Logistics Agency, Marrietta (K. Siler, Jr.)
1 Defense Nuclear Agency, Alexandria (Code LEEE)
1 Defense Nuclear Agency, Arlington (Code TDTR)
1 Defense Nuclear Agency (New Mexico Test Operations) Kirtland Air Force Base
  (Code TDNM-S)
2 Defense Technical Information Center, Alexandria, VA
3 Department of Defense Explosives Safety Board, Alexandria
  DDESB-IK (1)
  DDESB-KT (1)
  Dr. J. Ward (1)
1 Deputy Assistant Secretary of Defense (FSE&S)
1 National Security Agency, Fort George G. Meade (G74(TA)
1 Office of the Assistant Secretary of Defense (FM&P/SE&S)
4 Office of the Secretary of Defense
  ADDDR&E/T&E (TFR), D. French (1)
  ADDDR&E/T&E (SP), R. Ledsma (1)
  OUSDRE (OM) (1)
  USD(A)/DDRE(R&AT/ET), R. Menz (1)
2 Lawrence Livermore National Laboratory, Livermore, CA
  L-38, Military Applications (1)
  Technical Library (1)

3 Los Alamos National Laboratory, Los Alamos, NM
  Group M7, McAfee (1)
  Group M8, Asay (1)
  Technical Library (1)
2 Sandia National Laboratories, Albuquerque, NM
  Code 7553, M. Morris (1)
  Code 9122, R. Braash (1)
1 Advanced Technology, Incorporated, Arlington, VA
2 Aerojet Propulsion Division, Sacramento, CA
  Tactical Propulsion and Munitions, H. Whitfield (1)
  Tactical Systems, D. Snyder (1)
1 Aerojet Propulsion Division, Sacramento, CA (G. Manser)
2 Alliant Techsystems, Incorporated, Brooklyn Park, NM
  Dr. K. Christianson (1)
  K. Emerson (1)
1 Alliant Techsystems, Incorporated, Ridgecrest, CA
1 Applied Ordnance Technology, Incorporated, Arlington, VA
2 Atlantic Research Corporation, Virginia Propulsion Division, Gainesville, VA
  K. Grahm (1)
  Dr. R. Snyder (1)
1 Atlantic Research Corporations, Ridgecrest, CA (R. Miller)
1 BEI Defense Systems Company, Fort Worth, TS (W. S. Marks)
1 B. G. Craig Consultant, Energetic Materials, Niceville, FL
1 Boeing Aerospace Electronics, Ridgecrest, CA (G. Ebling)
2 Chamberlain Manufacturing Corporation, Waterloo, IO (J. Stotser)
1 Comarco, Incorporated, Weapons Support Division, Ridgecrest, CA (R. Dettling)
1 Denver Research Institute, University of Denver, Denver, CO
1 Fiest Engineering, Incorporated, Ridgecrest, CA
1 Hercules, Incorporated, McGregor, TX
1 IIT Research Institute, Chicago, IL (Technical Library)
1 Institute of Makers of Explosives, Washington, DC
1 Kilkeary, Scott & Associates, Incorporated, Arlington, VA
1 Lockheed Missiles & Space Company, Incorporated, Santa Cruz, CA (J. Farmer)
1 Lockheed Missiles & Space Company, Incorporated, Sunnyvale, CA (Ordnance Programs Office)
1 Martin Marietta Energy Systems, Incorporated, Oak Ridge, TN (D. Welch)
1 Martin Marietta Aerospace, Orlando, FL
1 Mason and Hanger, Amarillo, TX (A. G. Papp)
1 McDonnell Douglas Missile Systems Company, St. Louis, MO (Department E261)
1 Motorola, Incorporated, Scottsdale, AZ (Tactial Fuze Office)
1 Napadensky Engineers, Incorporated, Evanston, IL
3 New Mexico Institute of Mining and Technology, Socorro, NM
  L. Libersky (1)
  P. McLain (1)
  P. A. Persson (1)
1 Olin Ordnance, St. Petersburg, FL
1 Olin Ordnance, Washington, DC
1 Raytheon Company, Missile Systems Division, Bedford, MA
4 Southwest Research Institute, San Antonio, TX
  P. Bowles (1)
  W. Herrera (1)
  P. Zabel (1)
  Technical Library (1)
2 Tactical Product Engineering, Propulsion Division, Sacramento, CA
  R. Brogan (1)
  J. W. Jones (1)
1 The Johns Hopkins University, Applied Physics Laboratory, Laurel, MD
1 The Johns Hopkins University, Chemical Propulsion Information Agency, Columbia, MD
1 Thiokol Corporation/Huntsville Division, Huntsville, AL (W. Thomas)
1 Thiokol Corporation, Utah Tactical Division, Brigham City, UT
1 Thiokol Corporation, Wasatch Operations, Brigham City, UT (P. Nance)
1 Victor Technology, Ridgecrest, CA
1 VITRO, Washington, DC
1 Wyle Laboratories, El Segundo, CA (P. Turkheimer)
1 AWE Foulness Island, United Kingdom
1 CINO/DDEWS, Ministry of Defence, Bath, United Kingdom

2 Defense Research Establishment Valcartier, Quebec, Canada
C. Belanger (1)
J. F. Drolet (1)
1 DSTO/Materials Research Laboratory, Explosives Division, Victoria, Australia (M. C. Chick)
1 DSTO/Weapons Systems Research Laboratory, Ordnance Systems Division, Salisbury, Australia (L. Barrington)
1 Head of Research, Royal Ordnance Place, United Kingdom (Dr. P. R. Lee)
1 IETA Oliver Saliou, DGA/DCN Lorient, France
1 IJWA Boss van Charante, TDCK, The Netherlands
1 NATO Insensitive Munitions Information Center, Brussels, Belgium
1 RARDE/NP1, Waltham Abbey, United Kingdom
1 RARDE S/NP1 Division, Kent, United Kingdom
1 Royal Ordnance Rocket Motors Division, Worcestershire, United Kingdom
1 Sandy Smith, DRIC, Glasgow, United Kingdom